ChemComm

COMMUNICATION

View Article Online
View Journal | View Issue

Published on 21 December 2021. Downloaded by UNIVERSITE DE BORDEAUX on 7/11/2022 10:23:32 AM.

Check for updates

Cite this: *Chem. Commun.*, 2022, **58**, 1163

Received 29th October 2021,
Accepted 21st December 2021

DOI: 10.1039/d1cc06120h

rsc.li/chemcomm

Supramolecular gating of TADF process in self-assembled nano-spheres for high-resolution OLED applications†

Yu-Yu Hsieh,[ab] Rafael S. Sánchez,[c] Guillaume Raffy,[a] Jing-Jong Shyue,[d] Lionel Hirsch,[c] André Del Guerzo,[a] Ken-Tsung Wong *[b] and Dario M. Bassani *[a]

Acridine-based donor–acceptor chromophores exhibiting E-type delayed fluorescence were substituted with bis-biuret H-bonding motifs to induce the formation of hollow spheres which can be deposited from solution to form the active component of OLED devices. In solution, the contribution of the delayed component is sensitive to disruption of the aggregates.

Organic light-emitting devices (OLEDs)[1] have emerged as a leading technology for flat-panel display applications thanks to their high dynamic contrast, low power consumption, and compatibility with flexible substrates.[2] Compared to the use of rare-earth metal-based emitters, organic materials are abundant and allow tunable emission over the entire visible spectral range. Current research effort in this area is aimed at improving device efficiency, longevity, and resolution through careful design of the molecular components. A particularly important breakthrough is the harnessing of triplet states formed during charge recombination through the introduction of thermally-activated delayed fluorescence (TADF)[3–7] or the development of rt phosphorescent materials.[8–13]

In OLEDs, resolution is limited by cross-contamination between pixels of different colors due to efficient energy transfer in condensed materials. Compared to LCDs, OLEDs require a larger distance between pixels which limits high-resolution applications. Recently, we showed that the incorporation of hydrogen-bonding bis-biuret sites could be used to prepare emissive materials programmed to spontaneously self-assemble into well-defined hollow spheres in anhydrous organic solvents.[14,15] These are preserved upon drop-casting or spin-coating to generate individual pixels which can allow novel material properties, such as spontaneous self-sorting of different colors[16] and frequency-selective photobleaching.[17] Furthermore, we showed that individual spheres of each of the three primary colors could be deposited in very close proximity without bleeding or cross-contamination thanks to the pre-assembled supramolecular architectures.[14] These form pixels whose sub-micron size can, in principle, allow RGB resolutions attaining 20 000 dpi. However, the statistical formation of non-emissive triplet states contributes to the overall external quantum efficiencies (EQE) for these devices.

The design of TADF emitters rests on the near-degeneracy of the energies of the triplet and singlet states which allows thermal population of S_1 from the lower-lying triplet. Chromophores composed of a donor–acceptor pair allow separation of the wavefunctions of the singlet and triplet states, leading to a small singlet–triplet energy gap (ΔE_{ST}) conducive to TADF.[18] Along these lines, rigid emitters incorporating an acridine (donor) and a triazine (acceptor) possess emission quantum yields reaching 90% in doped films resulting in EQE > 25% in non-doped OLED devices.[19,20] The same acridine donor can be combined with a dicyano-substituted pyridine to tune the emission from green to yellow.[21] From our previous experience, introduction of biuret motifs at antipodal locations should result in the self-assembly of hollow spheres in which the H-bonding units are organized parallel to the surface of the sphere, as depicted in Fig. 1.

The propensity of the bis-biuret design to program the spontaneous self-assembly of vesicle-like hollow spheres even in the absence of aqueous media is remarkable and has proved to be robust towards different rigid or semi-flexible aromatic spacers. Herein, we show that the combination of a TADF chromophore with the directed self-assembly process imparted

[a] *Univ. Bordeaux, CNRS, Bordeaux INP, ISM, UMR 5255 F-33400 Talence, France. E-mail: dario.bassani@u-bordeaux.fr*
[b] *Department of Chemistry, National Taiwan University, and Institute of Atomic and Molecular Science, Academia Sinica, Taipei 10617, Taiwan. E-mail: kenwong@ntu.edu.tw*
[c] *Univ. Bordeaux, CNRS, Bordeaux INP, ENSCBP, IMS, CNRS UMR 5218, F-33400 Talence, France*
[d] *Research Center for Applied Sciences, Academia Sinica, Taipei 11529, Taiwan*

† Electronic supplementary information (ESI) available: Details of synthesis, aggregate characterization by fluorescence, transmission and electron microscopy, solvent polarity effects, device preparation, variable-temperature spectroscopy. See DOI: 10.1039/d1cc06120h

Published on 21 December 2021. Downloaded by UNIVERSITE DE BORDEAUX on 7/11/2022 10:23:32 AM.

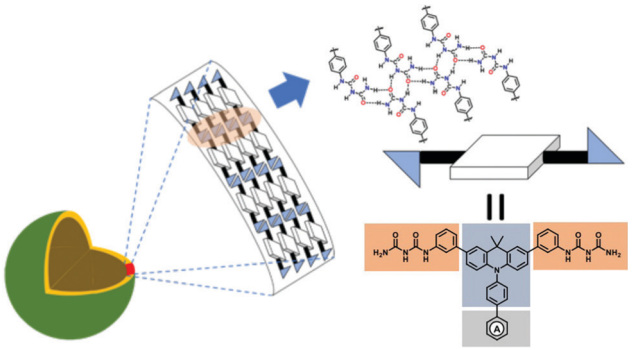

Fig. 1 Schematic representation of the self-assembly of nanospheres from donor–acceptor TADF chromophores possessing bis-biuret H-bonding motifs.

by the bis-biuret can lead to OLED materials with sub-micron sized emissive domains which exhibit TADF. Devices prepared from these materials show improved EQEs with respect to first-generation devices without TADF. Furthermore, we find that the bis-biuret unit acts as a quencher for the triplet state, but that this is impeded upon aggregation either in solution or in the solid. Therefore, chromophores involved in the formation of supramolecular aggregates will most benefit from TADF enhancement in a fashion that is reminiscent of the aggregation-induced emission of tailored flexible luminophores[22,23] and represents an example of TADF that is gated by supramolecular interactions.

The synthetic route to D–A chromophores composed of either a diphenyltriazine or dicyanopyridine acceptor and an acridine donor incorporating 2- or 3-phenylbiuret substituents is shown in Scheme 1 (see ESI† for full details). The phenylbiuret moiety was incorporated into the acridine unit by Suzuki–Miyaura coupling of the corresponding phenylboronic ester derivative. The *para* and *meta* isomers of compounds **1** and **2** are similar in their spectroscopic properties, with a weakly allowed S_0–S_1 transition at *ca.* 425 nm and a broad emission band in the visible region (Table 1 and ESI†). The solvatochromic behavior of the emission from ***m*-1** indicates that the excited state is considerably more polar than the ground state ($\Delta\mu$ = 22D), in agreement with strong charge-transfer character in S_1. Both **1** and **2** are strongly emissive in solution and in films, possessing bi-exponential decays with a long-lived μs component typical of compounds exhibiting E-type delayed fluorescence.

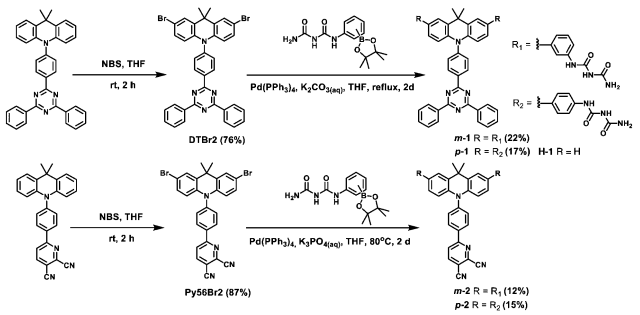

Scheme 1 Synthetic route to the *meta* and *para* derivatives of **1** and **2**.

Table 1 Summary of photophysical properties of **1** and **2**

	λ_{Abs}^{THF} (nm)	λ_{em}^{THF} (nm)	$\lambda_{em}^{tol.}$ (nm)	$\Phi_{THF}{}^{a}$	$\Phi_{tol.}{}^{a}$
***m*-1**	337	569	520	0.16 (0.074)	0.43 (0.18)
***p*-1**	339	576	525	0.11 (0.057)	0.37 (0.16)
***m*-2**	339	567	573	0.019 (0.013)	0.16 (0.062)
***p*-2**	334	566	578	0.017 (0.012)	0.10 (0.037)

[a] Emission quantum yield in degassed THF or toluene (tol.) 10^{-5} M solution, λ_{ex} = 350 nm. Values in parentheses correspond to aerated solutions.

In the case of ***m*-1**, the emission quantum yield in toluene solutions at r.t. is strongly dependent on the presence of oxygen. This behaviour is typical of TADF where the S_1 and T_1 excited states undergo partial equilibration.[24] Upon lowering the temperature, the proportion of E-type delayed fluorescence is decreased, in agreement with thermally-activated repopulation of S_1 (Fig. 2). By plotting the integrated intensities obtained from $A_i\lambda_i^{-1}$, where A_i and λ_i are respectively the pre-exponential factors and decay parameters from deconvolution of the time-resolved emission decay according to $I(t) = \sum_i A_i e^{-\lambda_i t}$, it is possible to obtain the relative proportions of the prompt (PF) and delayed (DF) fluorescence. Semi-logarithmic plots of λ_{DF} *vs.* T^{-1} yield straight lines from which the activation energy (E_a) for populating S_1 from T_1 can be extracted (Fig. 2 and Table 2). In all cases, E_a is sufficiently small for efficient thermal repopulation of S_1 at r.t. Switching from a low polarity solvent (toluene) to more polar THF leads to a small increase of E_a which reflects the relative solvent polarity stabilization of the T_1 *vs.* S_1 states.

In line with our previous findings,[25] scanning electron microscopy studies of glass substrates onto which dispersions of *para*- or *meta*- **1** or **2** (0.1 mM) in acetone, THF, or toluene were deposited *via* drop-casting or spin-coating revealed the presence of spheres 200–400 nm in diameter (Fig. 3).

Previous in-depth characterization of analogous architectures using DLS, small-angle X-ray scattering and cryo-TEM microscopy indicates that such architectures are present in solution and composed of a thin (*ca.* 10 nm thick) shell.[15] Their

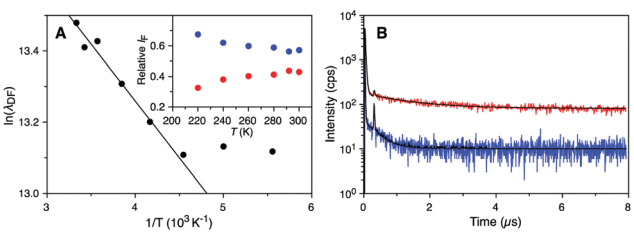

Fig. 2 (A) Arrhenius plot of the reciprocal of the long-lived decay component in the emission of ***m*-1** in degassed toluene solution. The straight line is the best fit through the 300–220 K region with E_a = 0.65 kcal mol^{-1} (r = 0.978). Inset shows relative contribution of the prompt (PF, blue) and delayed (DF, red) emission in the time-resolved decay. (B) Decay profile of the emission of ***m*-1** in degassed toluene solution (red) and degassed toluene/DMSO (10%) solution (blue). Black lines are non-linear best fit reconvolution according to bi-exponential functions with a short-lived component of 25.9 and 8.3 ns, and a long-lived component of 1.40 μs and 380 ns, respectively.

 This journal is © The Royal Society of Chemistry 2022

Published on 21 December 2021. Downloaded by UNIVERSITE DE BORDEAUX on 7/11/2022 10:23:32 AM.

Table 2 Activation energies and decay parameters[a] in THF and toluene

	E_a (kcal mol^{-1})		λ_{PF}^{-1} (ns)		λ_{DF}^{-1} (μs)	
	Toluene	THF	Toluene	THF	Toluene	THF
***m*-1**	0.65	0.98	25.9	20.0	1.40	0.64
***p*-1**	0.42	1.35	27.1	19.3	1.51	0.68
***m*-2**	—	0.78	25.0	20.1	1.09	1.61
***p*-2**	—	1.45	21.4	13.8	1.38	1.52

[a] In degassed solutions at 300 K.

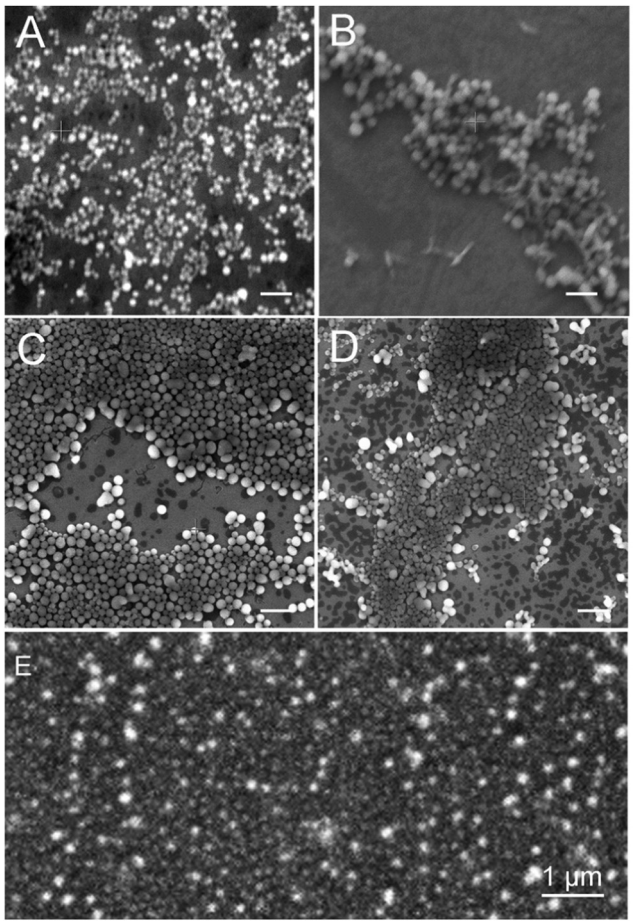

Fig. 3 SEM images of ***m*-1** (A), ***p*-1** (B), ***m*-2** (C), ***p*-2** (D) deposited by spin coating an acetone solution (0.1 mM) at room temperature (scale bar = 1 μm). (E) Confocal fluorescence microscopy image of a substrate coated with vesicles from ***m*-1** (λ_{ex} = 375 nm, λ_{em} = 420–470 nm).

stable emission is well-suited for hyperspectral imaging using confocal fluorescence microscopy which also evidences the formation of large areas covered by aggregates (Fig. 3E). Quantitative analysis of the emission intensity measured by luminescence microscopy suggests that the brighter aggregates may originate from solid spheres present in solution prior to deposition rather than from conglomerates of hollow spheres.

The addition of 10% DMSO (or MeOH) to a solution of vesicles of **1** or **2** in toluene or THF induces significant shortening of the long-lived component in the emission decay (from 1.40 μs to 380 ns in degassed toluene/DMSO (10%) solution). This is unexpected since neither solvent possess low-lying triplet states or redox properties that may quench the TADF process *via* energy or electron transfer. On the other hand, we have previously shown that both DMSO or MeOH induce disruption of the H-bonding of the bis-biuret derivatives and cause dissolution of the aggregates.[15] To understand the solvent dependence of the TADF chromophores, we prepared the corresponding model compound in which the biuret substituents are replaced by H (**H-1**, Scheme 1).[20] This compound exhibits similar excited-state decay parameters as ***m*-1** and ***p*-1**, with a long-lived contribution of 3.42 μs in toluene and 760 ns in THF. However, unlike ***m*-1** or ***p*-1**, the longer decay parameter is not significantly affected by the presence of 10% DMSO (630 ns in THF/10% DMSO). From this, we can deduce that the deactivation of the triplet state in **1** is dependent on the local environment: the shorter triplet lifetime in solution *vs.* film for **H-1** was previously assigned to vibronic coupling between the ground and excited state. A more polar solvent, such as THF, can decrease the energy of the excited state by stabilizing its charge-transfer character, thereby accelerating internal conversion. This suggests that the presence of the biuret substituents induces an additional non-radiative deactivation pathway (presumably though vibronic coupling)‡ which is turned off when the compounds are aggregated. Should this be confirmed, it would constitute an example of supramolecular gating of the TADF process in a fashion similar to that observed for AIE systems, where internal conversion to the ground state is impeded through aggregation.

To test whether TADF enhancement of OLED efficiency is compatible with supramolecular engineering of aggregate morphology, we proceeded to prepare devices incorporating compounds **1** and **2**. Previous proof-of-concept devices based on non-TADF materials exhibited low efficiencies (0.2–0.6%) due in part to the combination of non-productive charge recombination populating non-emissive triplet states.[14] To facilitate device fabrication, the use of a polymerizable hole transport layer was replaced by a host matrix selected based on the HOMO and LUMO energy levels of **1** and **2**.

The latter were determined from the onset of the absorption and emission spectra and the oxidation or reduction potential determined from electrochemistry (see ESI† for details on the calculation). Based on this, 4,4′-bis(*N*-carbazolyl)-1,1-biphenyl (CBP) was selected as a host matrix material to construct devices with an architecture composed of ITO/PEDOT:PSS/(**1** or **2**): CBP (0.2 : 1)/TPBi/LiF/Al. The absolute EQE curves averaged over 12 devices are shown in Fig. 4 along with wide-field electroluminescence microscopy image of a device prepared using ***m*-1** where it can be seen that the emission originates from submicron-sized aggregates identical to those imaged by photoluminescence. The results, collected in Table 3, evidence a notable improvement in device performance with respect to previous systems. As shown by the microscopy images of the device's electroluminescence, a portion of the active layer remains dark due to the absence of emissive aggregates. The interstitial area between aggregates may contribute to lowering the shunt resistance, which in turn limits the overall EQE measured over large active areas.

Published on 21 December 2021. Downloaded by UNIVERSITE DE BORDEAUX on 7/11/2022 10:23:32 AM.

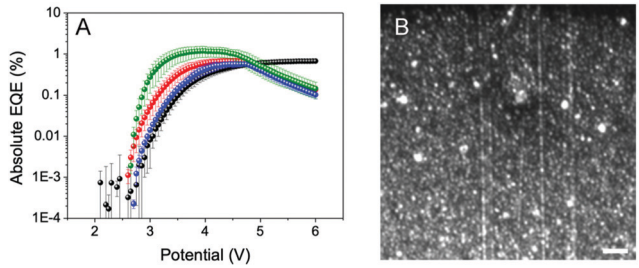

Fig. 4 (A) Absolute external quantum efficiency (EQE) *vs.* applied voltage of devices prepared from blends of ***m*-1** (black), ***p*-1** (red), ***m*-2** (blue), ***p*-2** (green) and CBP host (0.2 : 1) in THF. Each curve is the average of 12 devices. (B) Widefield microscope image of the electroluminescence from a device using ***m*-1** showing emission from the individual vesicles. Scale bar is 2 μm.

Table 3 Energy levels and electronic properties of **1** and **2**

	HOMO (eV)	LUMO (eV)	E_g (eV)	V_{ON} (V)	EQE (%@4 V)
***m*-1**	−5.60	−3.05	2.55	2.52	0.75[a]
***p*-1**	−5.58	−3.04	2.55	2.48	0.66
***m*-2**	−5.61	−3.32	2.29	2.54	0.60
***p*-2**	−5.59	−3.34	2.26	2.51	1.19

[a] Measured at 5 V

Our results lead us to conclude that TADF and supramolecular engineering of the active layer can be combined into OLED devices in which each aggregate acts as an isolated active area. This may facilitate the design of higher-resolution displays due to lower sensitivity to cross-contamination and spontaneous segregation of the individual pixels. Furthermore, we find that the contribution of the delayed component is decreased upon disruption of the aggregates.

This work was supported by the ANR (ANR-17-CE24-0033), the Ministry of Science and Technology, Taiwan project MOST 107-2923-002-001-MY3, and the IDEX University of Bordeaux. We are grateful to the CESAMO for structural analyses.

Conflicts of interest

There are no conflicts to declare.

Notes and references

‡ It is also possible that the difference in triplet lifetimes is due to differences in solvent polarity or localized solvation effects. However, we find that the long-lived decay of m-1 was only modestly reduced in neat acetone (to 1.08 μs). Acetone possess comparable polarity to neat MeOH and DMSO (ET(30) = 42.2, 45.0, and 55.5 for acetone, MeOH, and DMSO, respectively) but does not disrupt the formation of aggregates.

1 C. W. Tang and S. A. VanSlyke, *Appl. Phys. Lett.*, 1987, **51**, 913–915.
2 U. Mitschke and P. Bauerle, *J. Mater. Chem.*, 2000, **10**, 1471–1507.
3 A. Endo, M. Ogasawara, A. Takahashi, D. Yokoyama, Y. Kato and C. Adachi, *Adv. Mater.*, 2009, **21**, 4802–4806.
4 Q. Zhang, J. Li, K. Shizu, S. Huang, S. Hirata, H. Miyazaki and C. Adachi, *J. Am. Chem. Soc.*, 2012, **134**, 14706–14709.
5 F. B. Dias, K. N. Bourdakos, V. Jankus, K. C. Moss, K. T. Kamtekar, V. Bhalla, J. Santos, M. R. Bryce and A. P. Monkman, *Adv. Mater.*, 2013, **25**, 3707–3714.
6 U. Balijapalli, Y.-T. Lee, B. S. B. Karunathilaka, G. Tumen-Ulzii, M. Auffray, Y. Tsuchiya, H. Nakanotani and C. Adachi, *Angew. Chem., Int. Ed.*, 2021, **60**, 19364–19373.
7 C.-Y. Chan, M. Tanaka, Y.-T. Lee, Y.-W. Wong, H. Nakanotani, T. Hatakeyama and C. Adachi, *Nat. Photonics*, 2021, **15**, 203–207.
8 J.-H. Jou, S. Kumar, A. Agrawal, T.-H. Li and S. Sahoo, *J. Mater. Chem. C*, 2015, **3**, 2974–3002.
9 C.-Y. Kuei, W.-L. Tsai, B. Tong, M. Jiao, W.-K. Lee, Y. Chi, C.-C. Wu, S.-H. Liu, G.-H. Lee and P.-T. Chou, *Adv. Mater.*, 2016, **28**, 2795–2800.
10 M. Sarma, W.-L. Tsai, W.-K. Lee, Y. Chi, C.-C. Wu, S.-H. Liu, P.-T. Chou and K.-T. Wong, *Chem*, 2017, **3**, 461–476.
11 H. Sasabe and J. Kido, Eur, *J. Org. Chem.*, 2013, **2013**, 7653–7663.
12 K. Udagawa, H. Sasabe, C. Cai and J. Kido, *Adv. Mater.*, 2014, **26**, 5062–5066.
13 M. Mauro, *Chem. Commun.*, 2021, **57**, 5857–5870.
14 Y.-T. Tsai, K.-P. Tseng, Y.-F. Chen, C.-C. Wu, G.-L. Fan, K.-T. Wong, G. Wantz, L. Hirsch, G. Raffy, A. Del Guerzo and D. M. Bassani, *ACS Nano*, 2016, **10**, 998–1006.
15 S. K. P. Velu, M. Yan, K.-P. Tseng, K.-T. Wong, D. M. Bassani and P. Terech, *Macromolecules*, 2013, **46**, 1591–1598.
16 Y. T. Tsai, G. Raffy, H. F. Liu, B. J. Peng, K. P. Tseng, L. Hirsch, A. Del Guerzo, D. M. Bassani and K. T. Wong, *Mater. Chem. Front.*, 2020, **4**, 845–850.
17 Y.-T. Tsai, H.-F. Liu, B.-J. Peng, K.-P. Tseng, M.-C. Kuo, K.-T. Wong, G. Wantz, L. Hirsch, G. Raffy, A. Del Guerzo and D. M. Bassani, *ACS Appl. Mater. Interfaces*, 2017, **9**, 36045–36052.
18 Y. Wada, H. Nakagawa and H. Kaji, *Chem. – Asian J.*, 2021, **16**, 1073–1076.
19 W.-L. Tsai, M.-H. Huang, W.-K. Lee, Y.-J. Hsu, K.-C. Pan, Y.-H. Huang, H.-C. Ting, M. Sarma, Y.-Y. Ho, H.-C. Hu, C.-C. Chen, M.-T. Lee, K.-T. Wong and C.-C. Wu, *Chem. Commun.*, 2015, **51**, 13662–13665.
20 T.-A. Lin, T. Chatterjee, W.-L. Tsai, W.-K. Lee, M.-J. Wu, M. Jiao, K.-C. Pan, C.-L. Yi, C.-L. Chung, K.-T. Wong and C.-C. Wu, *Adv. Mater.*, 2016, **28**, 6976–6983.
21 I. S. Park, S. Y. Lee, C. Adachi and T. Yasuda, *Adv. Funct. Mater.*, 2016, **26**, 1813–1821.
22 J. Phelipot, N. Ledos, T. Dombray, M. P. Duffy, M. Denis, T. Wang, Y. Didane, M. Gaceur, Q. Bao, X. Liu, M. Fahlman, P. Delugas, A. Mattoni, D. Tondelier, B. Geffroy, P.-A. Bouit, O. Margeat, J. Ackermann and M. Hissler, *Adv. Mater. Technol.*, 2021, 2100876.
23 Y. Hong, J. W. Y. Lam and B. Z. Tang, *Chem. Commun.*, 2009, 4332–4353.
24 F. B. Dias, T. J. Penfold and A. P. Monkman, *Methods Appl. Fluoresc.*, 2017, **5**, 012001.
25 K. P. Tseng, F. C. Fang, J. J. Shyue, K. T. Wong, G. Raffy, A. Del Guerzo and D. M. Bassani, *Angew. Chem., Int. Ed.*, 2011, **50**, 7032–7036.

 This journal is © The Royal Society of Chemistry 2022